

Article

## Detecting Landscape Changes in High Latitude Environments Using Landsat Trend Analysis: 1. Visualization

Robert H. Fraser <sup>1,\*</sup>, Ian Olthof <sup>1</sup>, Steven V. Kokelj <sup>2</sup>, Trevor C. Lantz <sup>3</sup>, Denis Lacelle <sup>4</sup>, Alexander Brooker <sup>4</sup>, Stephen Wolfe <sup>5</sup> and Steve Schwarz <sup>6</sup>

<sup>1</sup> Canada Centre for Mapping and Earth Observation (CCMEO), Natural Resources Canada, Ottawa, ON K1S5K2, Canada; E-Mail: ian.olthof@nrcan.gc.ca

<sup>2</sup> Northwest Territories Geoscience Office, Yellowknife, NT X1A2L9, Canada; E-Mail: Steve\_Kokelj@gov.nt.ca

<sup>3</sup> School of Environmental Studies, University of Victoria, Victoria, BC V8W2Y2e, Canada; E-Mail: tlantz@uvic.ca

<sup>4</sup> Department of Geography, University of Ottawa, Ottawa, ON K1N6N5, Canada; E-Mails: dlacelle@uottawa.ca (D.L.); alex.brooker1@gmail.com (A.B.)

<sup>5</sup> Geological Survey of Canada, Natural Resources Canada, Ottawa, ON K1A0E8, Canada; E-Mail: swolfe@nrcan.gc.ca

<sup>6</sup> NWT Centre for Geomatics, Government of the Northwest Territories, Yellowknife, NWT X1A3S8, Canada; E-Mail: Steve\_Schwarz@gov.nt.ca

\* Author to whom correspondence should be addressed; E-Mail: robert.fraser@nrcan.gc.ca; Tel.: +613-694-2621.

External Editors: Santonu Goswami and Prasad S. Thenkabail

Received: 26 June 2014; in revised form: 31 October 2014 / Accepted: 4 November 2014 /

Published: 20 November 2014

---

**Abstract:** Satellite remote sensing is a promising technology for monitoring natural and anthropogenic changes occurring in remote, northern environments. It offers the potential to scale-up ground-based, local environmental monitoring efforts to document disturbance types, and characterize their extents and frequencies at regional scales. Here we present a simple, but effective means of visually assessing landscape disturbances in northern environments using trend analysis of Landsat satellite image stacks. Linear trends of the Tasseled Cap brightness, greenness, and wetness indices, when composited into an RGB image, effectively distinguish diverse landscape changes based on additive color logic. Using a variety of reference datasets within Northwest Territories, Canada, we show that the

trend composites are effective for identifying wildfire regeneration, tundra greening, fluvial dynamics, thermokarst processes including lake surface area changes and retrogressive thaw slumps, and the footprint of resource development operations and municipal development. Interpretation of the trend composites is aided by a color wheel legend and contextual information related to the size, shape, and location of change features. A companion paper in this issue (Olthof and Fraser) focuses on quantitative methods for classifying these changes.

**Keywords:** arctic; change detection; image stacks; disturbance; lakes; slumps; fires; environmental monitoring; cumulative impacts

---

## 1. Introduction

Northern environments are changing rapidly in response to recent climate warming, human development, and natural disturbances [1]. Monitoring these environments to inform decision makers and land and wildlife managers poses significant challenges due to their large extent and sparse human populations. Canada's northern territories (Yukon Territory, Northwest Territories, and Nunavut) cover 39% of the country, but contain only 0.3% of its population. Nevertheless, northern Aboriginal peoples are closely tied to the land, and are greatly impacted by changes to the ecosystems on which they depend.

Environmental monitoring in Canada's North has mainly been conducted at local scales through the use of aerial reconnaissance and photography, and field-level ecological, hydrologic, and geologic sampling and surveying [2]. Satellite remote sensing offers a complementary, cost-effective tool for spatially comprehensive northern monitoring but at a coarser spatial resolution. Remote sensing has successfully been used to detect and map large-area landscape changes related to Arctic lake extent [3,4], storm-surge vegetation dieback [5], glacier retreat [6], vegetation greening [7], and forest fires [8–10] over Canada's North.

The opening of the USGS Landsat archive in 2008 for free data access, combined with the Landsat Global Archive Consolidation initiative, has facilitated the development of new change detection methods that exploit temporally dense collections of imagery (image stacks). These methods quantify pixel-level spectral trajectories through time by fitting parametric functions [11,12], temporally segmenting spectral index values [13], detecting anomalous deviations in a time series that are indicative of disturbance or land cover change [14], or applying a dynamic and continuous time series model based on seasonality, trend, and breaks [15]. To date, most of the Landsat trajectory methods have been applied to temperate regions to characterize disturbance and recovery of forested ecosystems, while relatively few have examined northern environments [16–21]. A major advantage of applying image stack approaches in the North compared to conventional two-date change detection is a greater ability to distinguish subtle, long-term changes, such as Arctic greening or drying of lakes, from changes caused by inter-annual climate variations [20,21].

The purpose of this research is to investigate the range of northern landscape changes that can be detected using Landsat trend analysis. These changes relate to natural disturbances such as forest and tundra fires, tundra greening, and fluvial processes; geomorphic disturbances such as gradual and catastrophic lake drainage and retrogressive thaw slumping; and anthropogenic changes related to

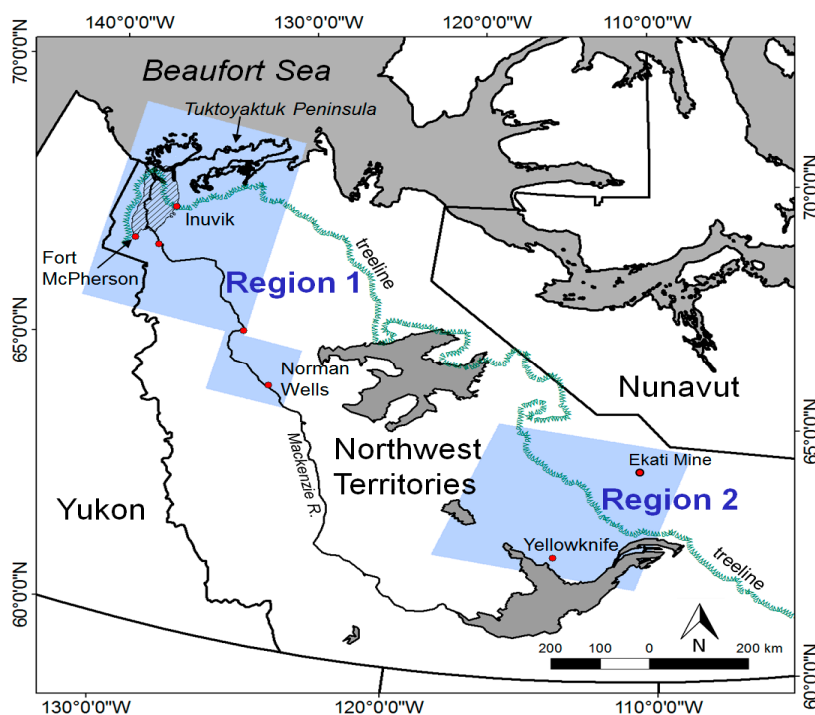
northern development. We describe a simple, yet highly effective technique to visualize these changes based on color compositing of linear trends computed from dense stacks of Landsat imagery. The method, dubbed Landsat Arctic Rgb CHanges (LARCH) is underpinned by a quantitative analysis of Landsat image stacks, but the output is an image designed for visual analysis in a GIS environment. In this paper, we demonstrate the application of LARCH using examples derived from multiple spatial and temporal scales, and environments across the Northwest Territories (NWT). The scientific and applied significance as well as potential future research directions are addressed for several of these cases.

## 2. Methods

### 2.1. Study Regions

Stacks of near-annual Landsat imagery were processed for two study regions in the NWT covering about 300,000 km<sup>2</sup> or 22% of the territory (Figure 1 [22]). Region 1 extends from the town of Norman Wells to the Tuktoyaktuk Peninsula. Region 2 covers NWT's zone of major mining activity and extends from the city of Yellowknife to the Ekati diamond mine. Together, the study areas encompass four of the major ecological regions in the NWT (Taiga Shield, Taiga Plains, Taiga Cordillera, and Southern Arctic Tundra Plains), which transition from high-boreal forest to low-arctic tundra above treeline [23]. Both regions are underlain by permafrost: continuous permafrost occurs throughout most of the more northerly region 1, whereas extensive discontinuous permafrost is found in region 2 and in an area around Norman Wells in region 1. The regions contain numerous shallow lakes that cover 18% of the study areas.

**Figure 1.** Two study regions analyzed using Landsat TM/ETM+ satellite imagery from 1985 to 2011. The treeline was digitized from Timoney *et al.* [22] and represents the 1:1 tree:upland tundra cover isoline.



This region has experienced rapidly warming air temperatures during the past 50 years at a rate that is four to five times the global average. This 2.0–2.7 °C temperature increase has warmed permafrost [24,25], accelerated thermokarst processes [26], impacted the stability of infrastructure, and altered tundra ecosystems [27]. The Northwest Territories has also seen an intensification of resource development activity related to hydrocarbon exploration (region 1), diamond mining (region 2), and the growth of community and transportation infrastructure (regions 1 and 2). These pressures and the cumulative impacts they create underscore the need to expand the scope and scale of environmental monitoring within the NWT [2,28].

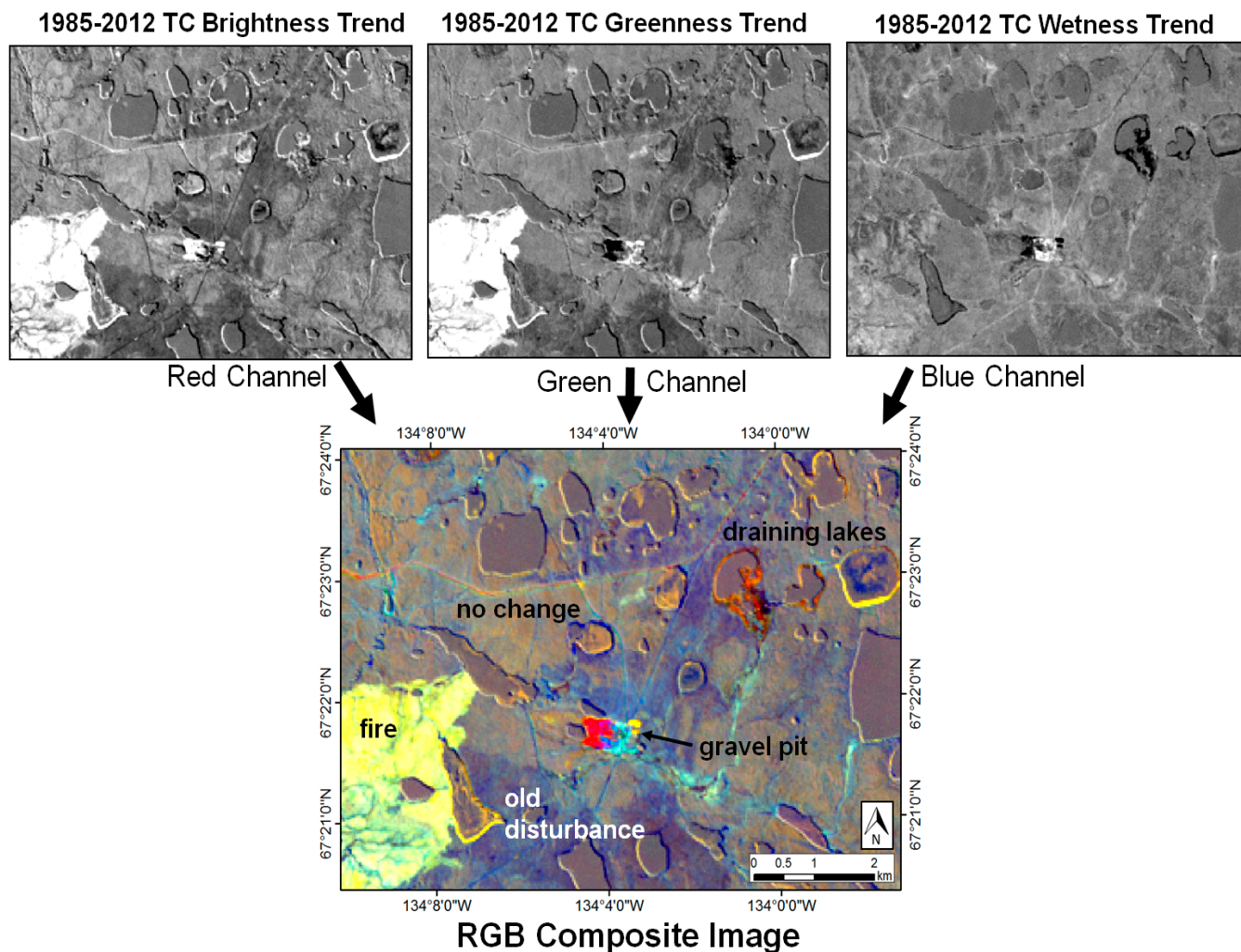
## 2.2. Landsat Imagery

Candidate July–August growing season images from 1985 to 2011 were identified from 26 overlapping WRS-2 frames using the US Geological Survey’s Glovis data portal (<http://glovis.usgs.gov>). A total of 234 level-1 terrain corrected Landsat TM and ETM+ images were calibrated to top-of-atmosphere reflectance using USGS coefficients [29], and screened for cloud and cloud shadow using the methods described in Fraser *et al.* [17]. Missing scan line data in ETM+ images after the 2003 scan line corrector failure were masked and treated as cloud. This resulted in image stacks with an average of 17 clear-sky observations per pixel from the July–August growing season. The Tasseled Cap (TC) Brightness, Greenness, and Wetness indices were then derived using coefficients provided by Crist and Cicone [30]. The TC indices are based on orthogonal, linear combinations of Landsat channels 1 to 5 and 7. TC Brightness (TCB) is computed from a weighted sum of all six TM/ETM+ reflectance bands, TC Greenness (TCG) contrasts the visible and near-infrared bands and is correlated to green leaf area, and TC Wetness (TCW) contrasts the short-wave infrared with all other channels and is related to soil and canopy moisture. Linear trends in the three TC indices were computed for each 30 m pixel (ignoring screened pixels) using TheilSen non-parametric linear regression, which is calculated as the median of all possible pairwise slopes and is insensitive to up to 30% of outliers [31]. Significant slopes, evaluated using the rank-based Mann-Kendall test, represented TC change per day since the first Landsat observation in 1985. Our visualization method utilizes the 32-bit output regression slopes (trends) that are converted to scaled, 16-bit images for RGB compositing.

## 2.3. Landsat RGB Trend Compositing

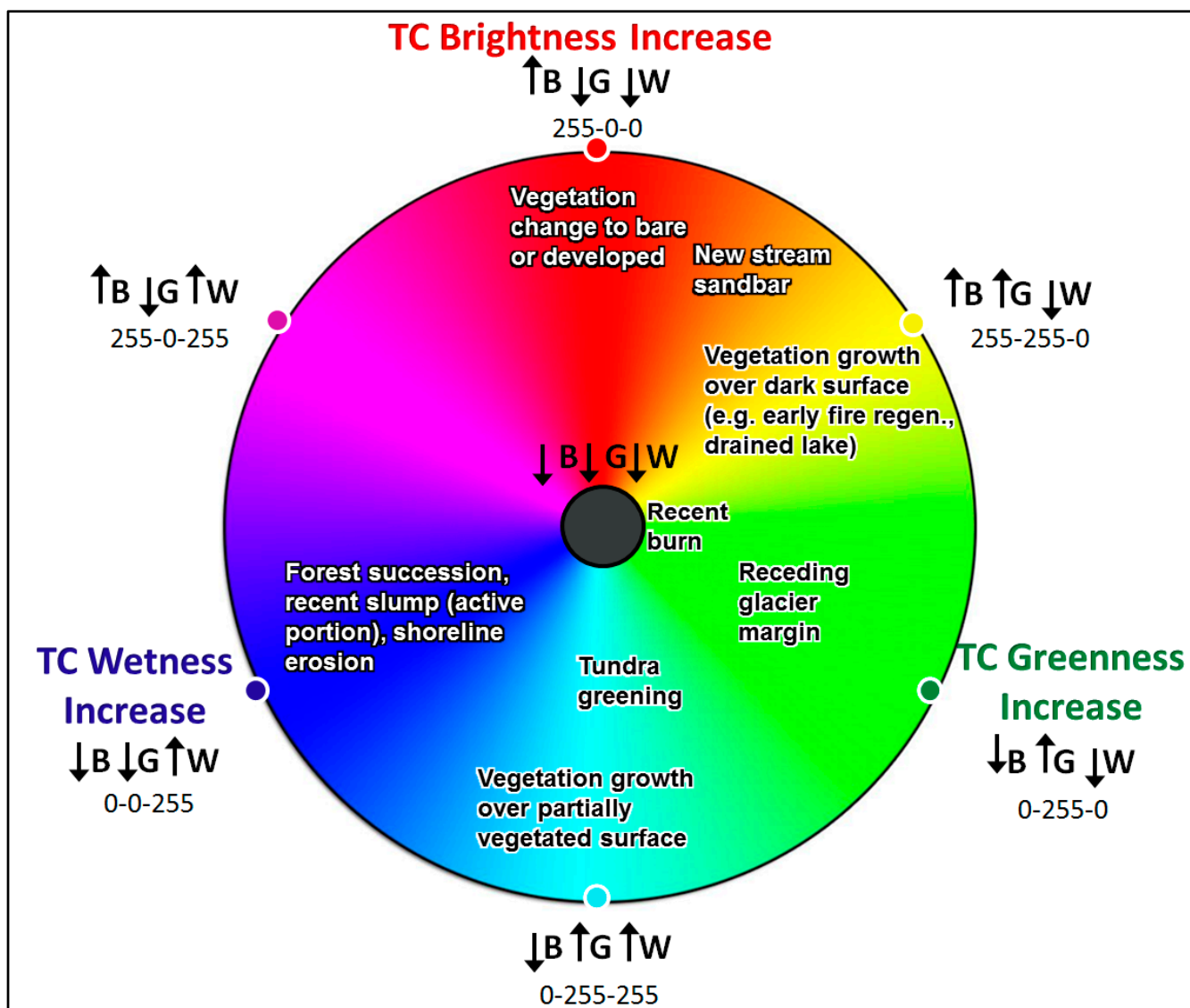
Each TC linear trend (or slope) image indicates the direction (light = increasing, dark = decreasing) and magnitude of spectral changes in pixel brightness (TCB), greenness (TCG), and wetness (TCW) (Figure 2). The key feature of the LARCH method is that the three TC trends are composited into a contrast-stretched RGB image so that the three-dimensional TC trajectory can be visualized using additive color logic (Figure 2). Image compositing was accomplished using the Composite Bands tool in Esri ArcGIS 10.1 and the resulting RGB-TIFF images were visualized in Esri ArcMap 10.1 based on a linear histogram stretch to a range of plus or minus two standard deviations.

**Figure 2.** Tasseled Cap (TC) trend compositing method used by LARCH. Individual trend (slope) images from linear regression analysis of the Landsat image stack are composited as an RGB image to yield unique colors representing the three-dimensional TC trajectory.



Effectively, this method is an extension of RGB overlay of image channels or vegetation indices from two or three image dates used previously to highlight land cover changes (reviewed in [32]). The LARCH method can be used to identify a wide range of natural and anthropogenic landscape change processes unique to northern environments based on differences in TC trend signatures. An RGB color wheel showing all combinations of increasing and decreasing TC trends provides a legend that highlights the major types of landscape changes (Figure 3). As we demonstrate with the case studies discussed in this paper, a combination of the TC indices in RGB space and contextual information related to the shape, size, and location of change objects can be sufficient to identify the type of landscape change without the benefit of ground-based information. This visual approach is therefore well-suited for application to large, remote areas where ground-based monitoring would otherwise be expensive and logistically challenging.

**Figure 3.** Color wheel legend showing the major types of landscape changes that can be interpreted from RGB compositing of the linear TC trends. The changes in each TC index that characterize each color family are shown on the outside of the color wheel.



#### 2.4. Reference Data

Since the change products generated using this procedure are qualitative and visual, this precludes a conventional, statistical validation of them. Instead, we conducted a comprehensive investigation and corroboration of the TC trend images using air photos, fire surveys, and other GIS databases (Table 1). We also investigated a range of features visible in the trend images by capturing oblique photos during 2011–2013 helicopter flights in areas around Yellowknife, Fort McPherson, and between Inuvik and Tuktoyaktuk. Interpretation of the trend composites is facilitated by knowledge of the spectral expression of physical and biological changes caused by different disturbance mechanisms. In the next section, we present and discuss a broad range of RGB TC change trajectories occurring within the two large study regions.

**Table 1.** Reference data used to identify and corroborate landscape changes observed in the Landsat Tasseled Cap trend imagery.

Data Set	Description	Types of Change Features Corroborated
Mackenzie Valley Orthophotos (MVAP)	Contracted by Indian and Northern Affairs Canada, photos are from August 2004, 1:3000 scale, ~1 m resolution	Slumps, drained lakes, seismic lines
NWT Community Orthophotos	Acquired by NWT Department of Municipal and Community Affairs in 2007–2012, 5 cm resolution	Footprint and type of municipal development
SPOT Imagery	2005–2010 SPOT 4&5 imagery processed by NWT Centre for Geomatics, pan-fused 10 m resolution	All
Landsat TM and ETM+ imagery	Visual interpretation of 1985 and 2011 image pairs used to generate image stacks	All
Fire History of NWT	NWT Department of Environment and Natural Resources, 1965–2011 burned area polygons	Post-1965 forest fires
National Air Photo Library photographs	Panchromatic photographs 1950–1985, scales of 1:5000+	Pre-1965 forest and tundra fires, thaw slump progression, drained lakes
Ecological Land Classification (ELC) oblique air photos	NWT Department of Environment and Natural Resources, > 60,000 oblique aerial photographs from 2005 to 2009	All
Vertical color and color-infrared air photo pairs	208 vertical air photos pairs from 1980 and 2013, ~2–4 cm effective resolution, 14 flight lines over Tuktoyaktuk Peninsula (Fraser <i>et al.</i> [21])	Shrub proliferation
Oblique air photos from helicopter	Photos taken around Ft McPherson and between Inuvik and Tuk, August 2013, and around Yellowknife, August 2011 and June 2012	All
Google Earth	Areas containing high resolution (<4 m) imagery	All
National Hydro Network	Lake perimeters and stream networks at 1:50,000 scale compiled by Natural Resources Canada	Draining lakes, thaw slumps
Peel Plateau thaw slumps	212 digitized slumps	Retrogressive thaw slumps
NWT Seismic Lines	Historical seismic line GIS database from National Energy Board	Seismic line disturbances
NWT Spatial Data Warehouse	Geospatial Portal containing numerous NWT spatial datasets	Mineral, oil, and gas developments

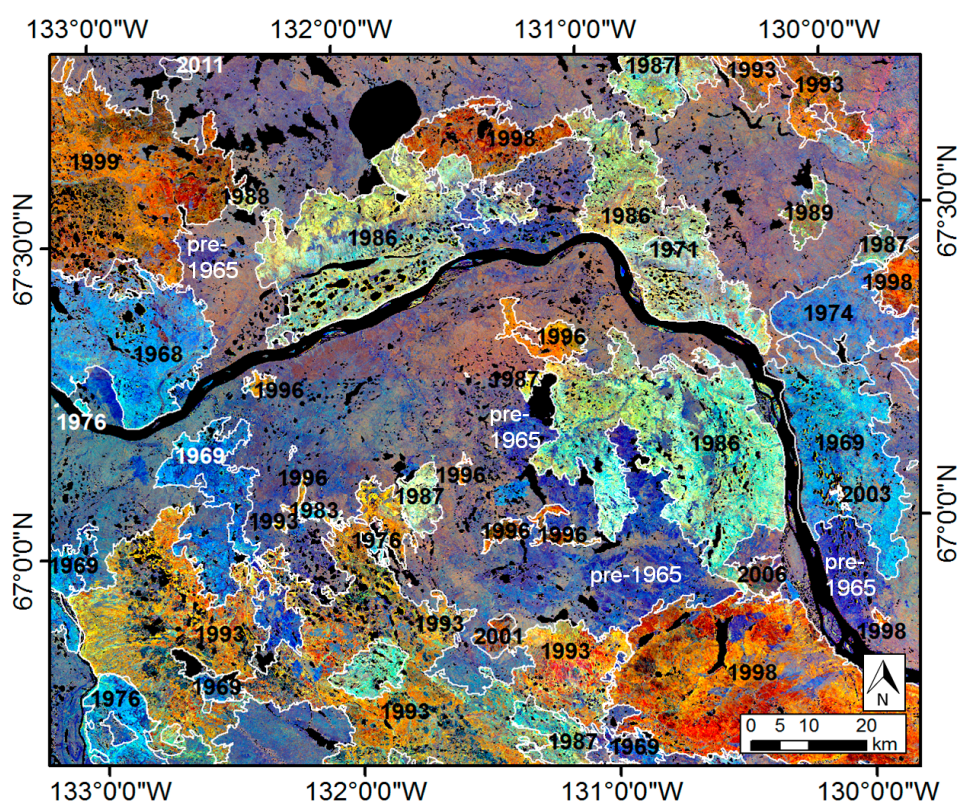
### 3. Results: Types of Landscape Changes Observed

#### 3.1. Wildfires

Wildfires are the dominant disturbance impacting the boreal forest in NWT. Regenerating fires were also the most common change feature in the TC trend images, as the NWT fire database indicates that 22% of the study regions have been impacted by fire since 1965. Figure 4 shows fire history perimeters overlaid on the trend image for a region with frequent fire return interval surrounding the lower Mackenzie River. The extent of vegetation recovery and post-fire successional stages are clearly visible

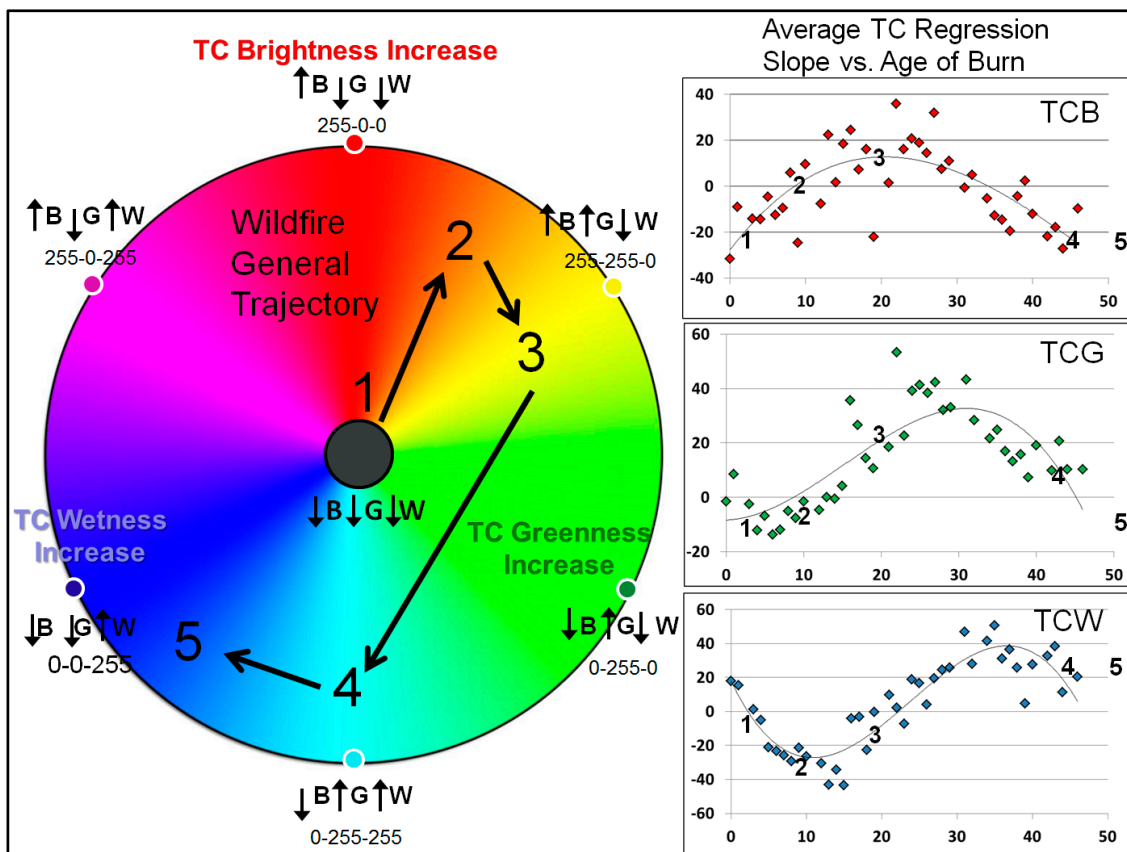
in the RGB TC trend space shown in Figure 4. The RGB changes associated with this successional trajectory are shown in Figure 5: Recently burned forest appears dark (1), then brightens to orange and yellow with expanding broadleaf cover (2–3). Gradual forest crown closure and succession towards needle-leaf species results in stands that appear in blue (4–5). Note that very recent fires (e.g., the 2011 fire in the upper portion of Figure 4) have a flat trajectory for all but one or few data points. These values are typically treated as regression outliers and therefore recent disturbances are not normally visible in the trend images.

**Figure 4.** NWT fire history perimeters (1965–2011) overlaid on the TC trend image composite. Regenerating stands initiated by fires before 1965 appear dark blue.



It is likely that variation in TC slope trajectories among fires with similar burn dates (Figure 5 right) is related to differences in burn severity, regeneration rates, and species composition of forest stands during succession [33,34]. Although fires with similar ages have similar TC slope trajectories, the interpretation of linear trajectories is complicated by the fact that the overall spectral trajectory of burned forest through vegetation succession is non-linear [35]. The use of linear slopes to characterize such non-linear trajectories is therefore a simplification, but nonetheless generates a predictable and useful output composite RGB image. As we show in our companion paper, non-linear regression coefficients and template matching based on temporal profile shape and distance were not optimal for classifying disturbance types. Rather, robust linear TC trend coefficients were found to be most effective for classification of change type [36].

**Figure 5.** General trajectory of regenerating wildfires in RGB trend space from recently burned forest (1), expanding broadleaf cover (2–3) and succession towards needleleaf species (4–5). Also shown are the linear regression TC slopes averaged by age of burn with third-order polynomial curves overlaid to show the shape of the trajectories. The three TC slope values on the graphs are combined to generate the RGB colour trajectory (left) labelled as 1–5.



One of the most interesting applications of the LARCH method is the ability to detect evidence of fires occurring before the 1965 start of the NWT fire database. These regenerating burns appear dark blue as a result of long-term succession from a vegetation cover dominated by broadleaf shrubs and trees to one dominated by needleleaf trees that have a lower brightness and greenness (Figure 4). Figure 6 shows the trend image for a stand regenerating from a pre-1965 fire adjacent to a mature conifer forest where there is no significant TC trend (generating grey tones). We were able to verify that many of these dark blue TC trend patches are pre-1965 fires by examining forest composition in recent oblique air photos and by comparing pairs of historical, vertical air photos.

Very large patches of regenerating vegetation resulting from pre-1965 fires in spruce woodlands and tundra are also visible near the treeline (Figure 7). The perimeters of these two fire complexes were sketched in Cody [37], who identified them as having occurred in 1954. These regenerating patches are estimated to cover 2031 km<sup>2</sup>, making them twice the size of the unprecedented 2007 Anuktuvuk River fire in Alaska that burned 1039 km<sup>2</sup> of tundra [38]. Also detectable are smaller treeline burns in both study regions not included in the NWT fire history, four of which could be dated to 1989 (Figure 7) using single Landsat scenes.

**Figure 6.** TC trend composite image (**top left**) showing the boundary between a mature forest and stand initiated following a pre-1965 fire, which is also observable in a 2006 SPOT Image (**top right**). The broadleaf-needleleaf composition of forest in the area is visible in a recent oblique air photo captured by the NWT Government (**bottom**). The small arrow shows the direction from which the photo was taken.

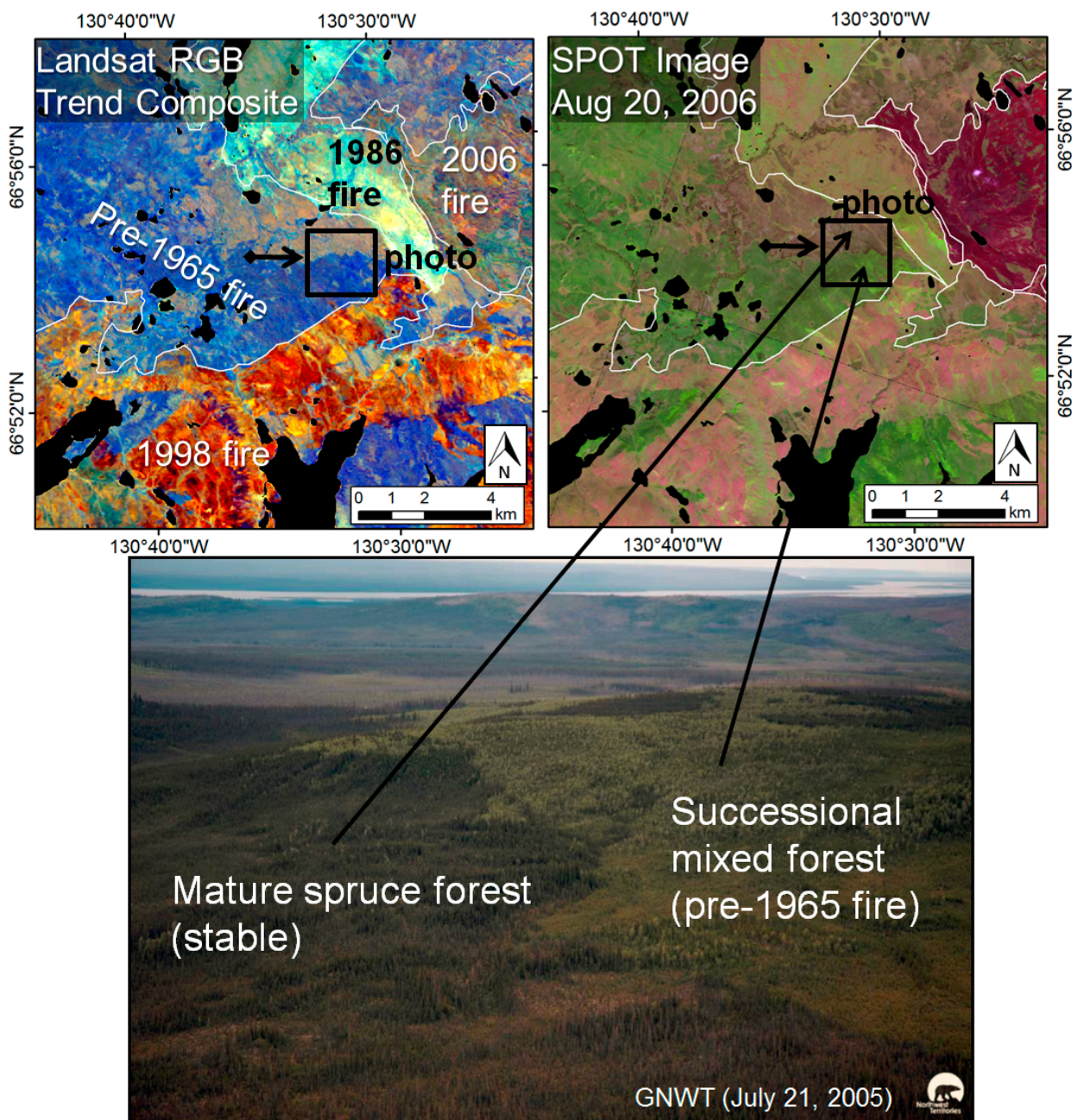
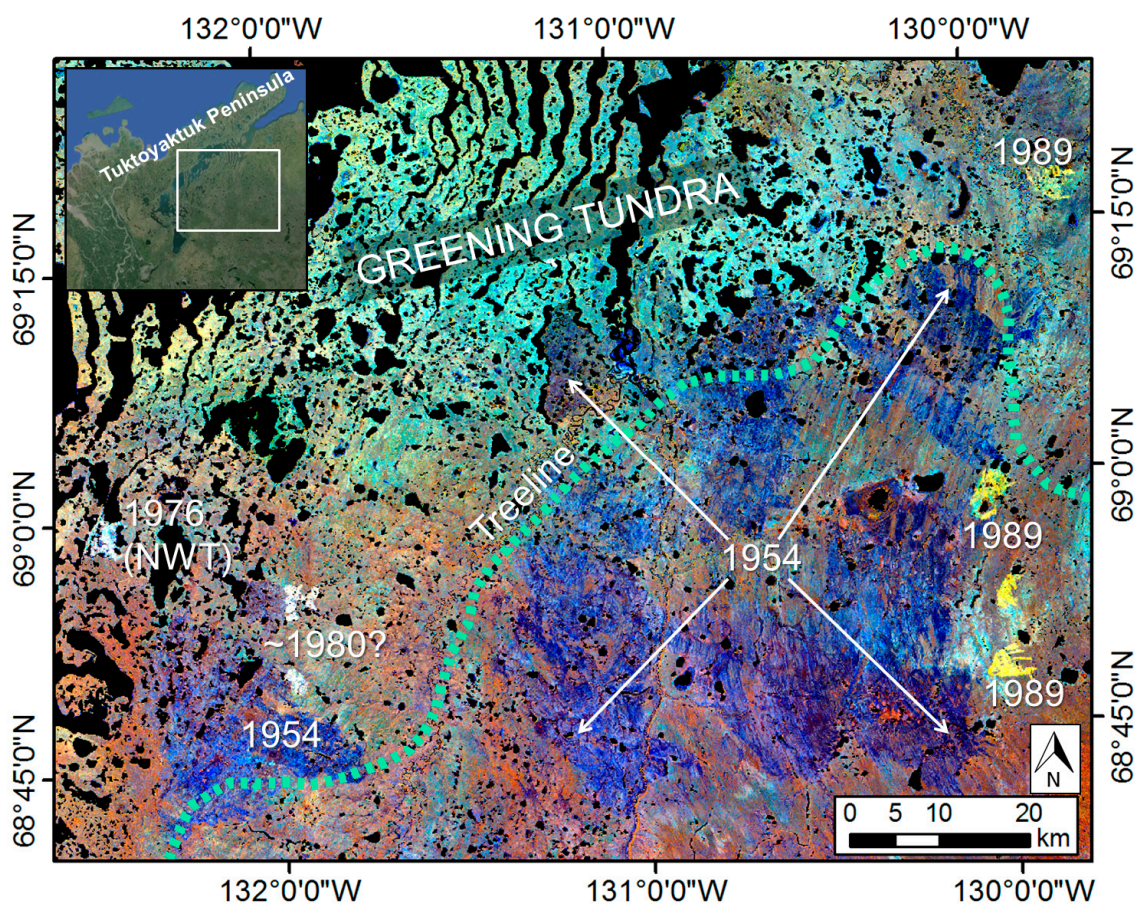


**Figure 7.** Area along the treeline in study region 1 containing large regenerating fire complexes, which burned in 1954 (dark blue color). Also observable are smaller, more recently regenerating burns (light and yellow colors) with year of burning indicated and greening tundra vegetation (teal color). The 1976 tundra burn is included in the NWT fire history survey. The treeline was digitized from Timoney *et al.* [22] and represents the 1:1 tree:upland tundra cover isoline.



### 3.2. Tundra Greening

The greening of Arctic tundra, primarily as a result of warming-induced shrub proliferation, has been widely observed in northern ecosystems [39]. Studies using coarse resolution (>1 km) NOAA AVHRR satellite imagery have shown that the northern portion of study region 1 has undergone greening since 1985 [7,40,41]. These changes are also observable in the higher resolution trend composites as a teal color, indicating a surface that is becoming greener and wetter due to increasing leaf biomass (Figure 7).

A recent investigation of these greening changes using the same 1985–2011 Landsat image stack showed that the Tuktoyaktuk Peninsula has significant positive NDVI trends (strongly related to TCG) over 85% of its land area [21]. A comparison of 208 high resolution vertical air photo pairs from 1980 and 2013 indicated that regional greening was primarily a result of expanding cover of dwarf and tall shrubs, with a concurrent decline in lichen cover. These broad-scale vegetation changes have implications for ground thermal conditions and permafrost stability, tundra wildfire activity, and availability of winter lichen forage for caribou [21,27] as well as global implications for climate due to a reduction in surface albedo [42].

### 3.3. Lake Surface Area Changes

Several recent studies have used time series of Landsat imagery to quantify changes in the area of Arctic lakes [3,4,20,43,44]. Arctic and sub-arctic lakes surrounded by ice-rich permafrost are susceptible to expansion by thermokarst processes, which may sometimes lead to catastrophic drainage [26,45]. Lakes may also drain into the groundwater system as subsurface pathways expand with permafrost degradation and talik expansion [46]. In areas with shallow lakes, changes in the annual water balance may lower water levels, decrease lake surface area and expose lake beds [3]. Lake drainage initiates a successional sequence that is dictated by several factors including latitude, nature of lake-bottom sediments, and whether or not permafrost aggrades into the exposed sediments. Aggradation of permafrost can heave lake-bottom sediment, lead to thermal contraction cracking and development of polygonal terrain, and in extreme cases result in pingo development (a periglacial landform consisting of earth-covered ice), as observed in the Tuktoyaktuk Peninsula [47].

The expansion of lakes due to shoreline erosion is visible on LARCH composites in both study regions, and is common within lowland areas west of Yellowknife and portions of the Tuktoyaktuk Peninsula (Figures 8–10). These changes appear dark blue in the trend image owing to a darker, wetter, and less vegetated surface. Many of these changes also appear to be related to ponding of surface water (Figure 8), which is likely the result of thermokarst within the ice-rich terrain (e.g., ice-wedge polygons) [48,49] and/or long-term increases in precipitation [3]. Inspection of single Landsat images from the time series indicates that these 1985–2011 changes are generally gradual and unidirectional. Erosion along the Beaufort Sea coastline shows a similar trajectory to lake expansion (Figure 8) and occurs throughout region 1. Retreat rates along the Tuktoyaktuk Peninsula averaged 0.7 m/yr during 1985–2000, but were as high as 9 m/yr in some areas [50] making the changes easily observed using a 26-year collection of 30 m imagery.

Draining or drying lakes that have been colonized by graminoid and shrub vegetation are also visible in the trend images throughout both study regions as yellow tones, representing a brighter, greener, and drier surface, which is the opposite trend shown by expanding lakes. Corroboration that these trends are associated with lake drainage/drying comes from both recent oblique aerial photos and by overlaying lake boundaries from the National Hydro Network database showing historical (~1950) lake extents (Figure 9). Drained lakes were also observed within previously burned areas along the Mackenzie River, resulting from the removal of insulating organic materials and permafrost warming [44] (Figure 9). Many of the bays and wetlands along the northern shoreline of Great Slave Lake also showed evidence of vegetation growth over the formerly dark water surface (Figure 10). These changes are likely due to a ~20 cm drop in water levels during the 1985–2011 analysis period (Figure 10).

**Figure 8.** Area east of Tuktoyaktuk showing widespread increases in wetness in the trend image (**top**) over ice-wedge polygon terrain (dark blue), some expanding lakes (dark blue), and eroding coastline (dark blue and red). Areas of surface ponding can be observed in recent oblique air photos captured by the NWT Government (**bottom**). The red arrows show the direction from which the photos were taken.

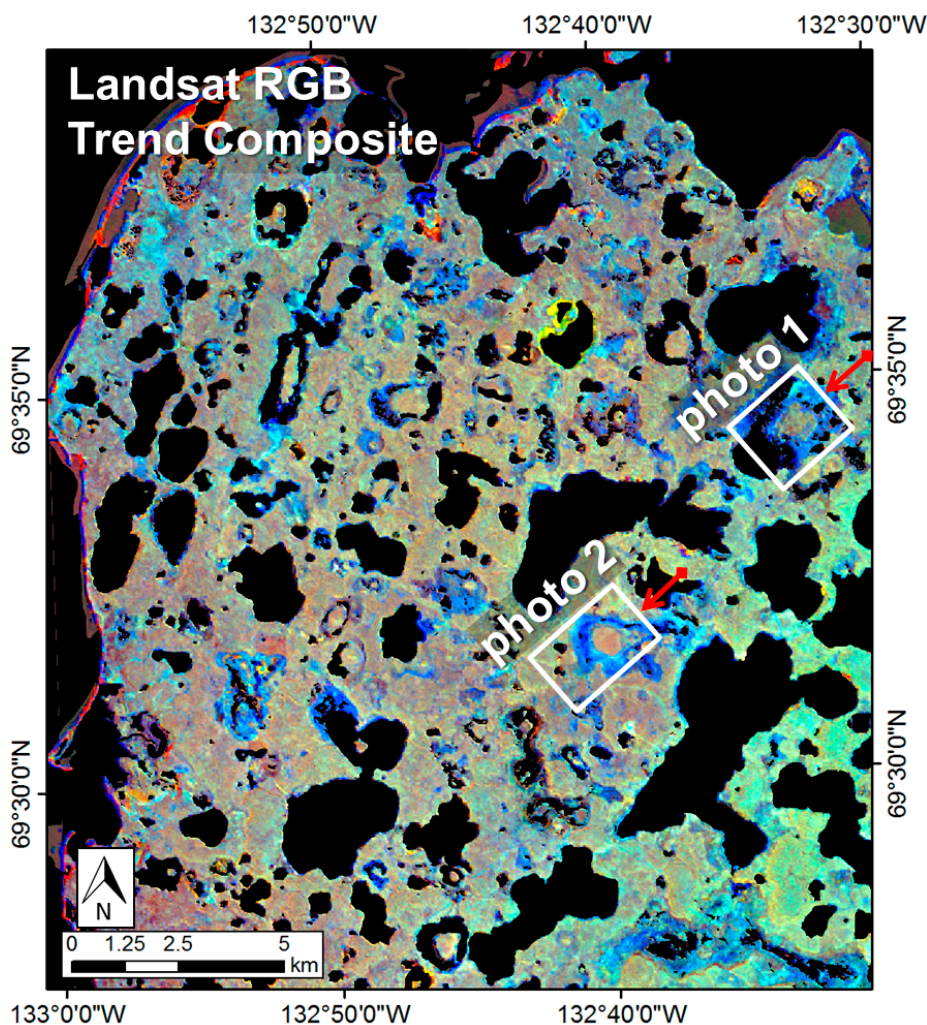


**Figure 9.** TC trend image (**top**) showing draining or drying of shallow lakes (yellow) within a 1986 burn. Historical lake perimeter from the National Hydro Network are overlaid showing ~1950 lake extents. Exposed and vegetating lake beds are visible in recent oblique air photos from the NWT Government (**bottom**). The red arrow shows the direction from which the photo was taken.

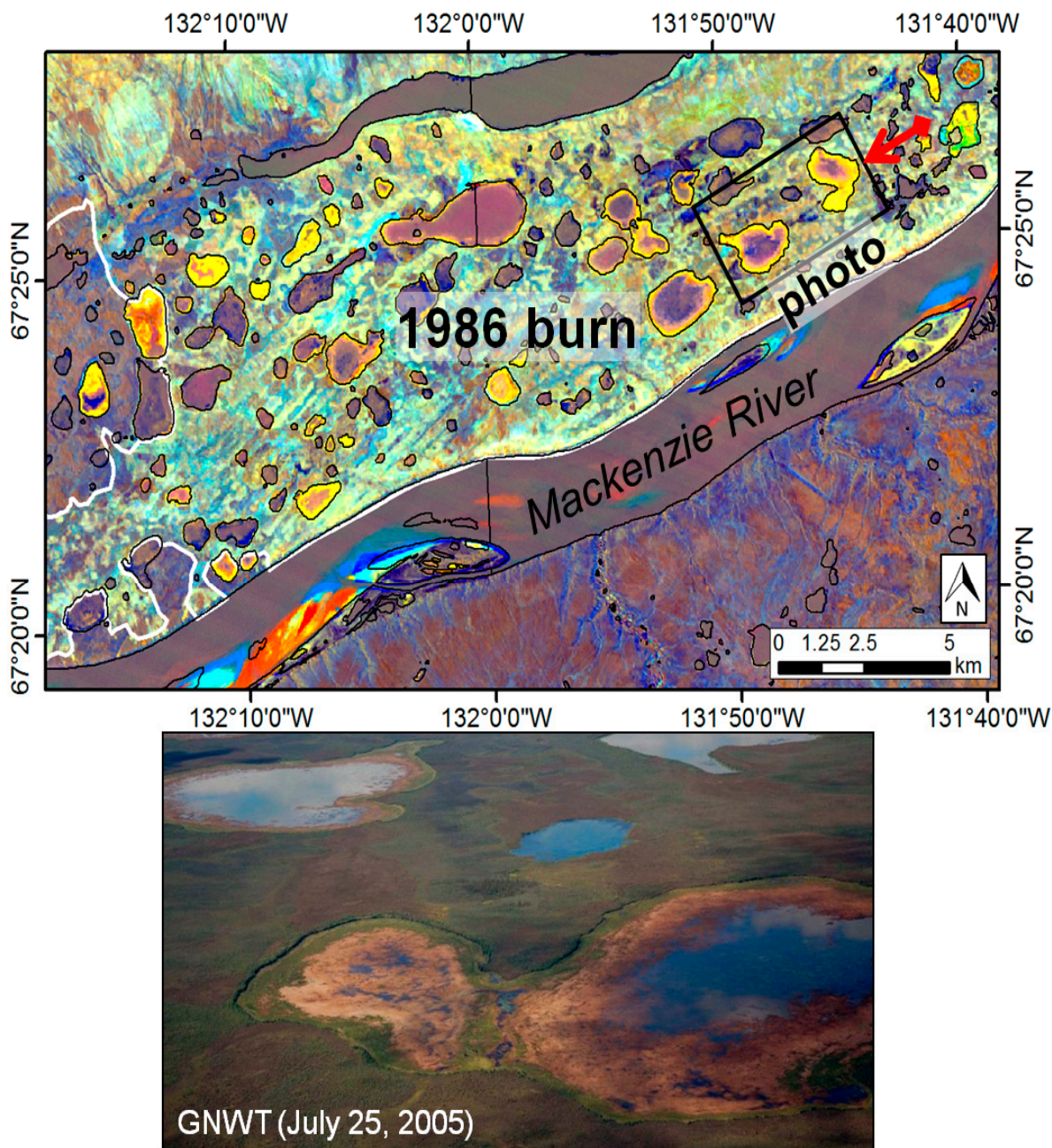
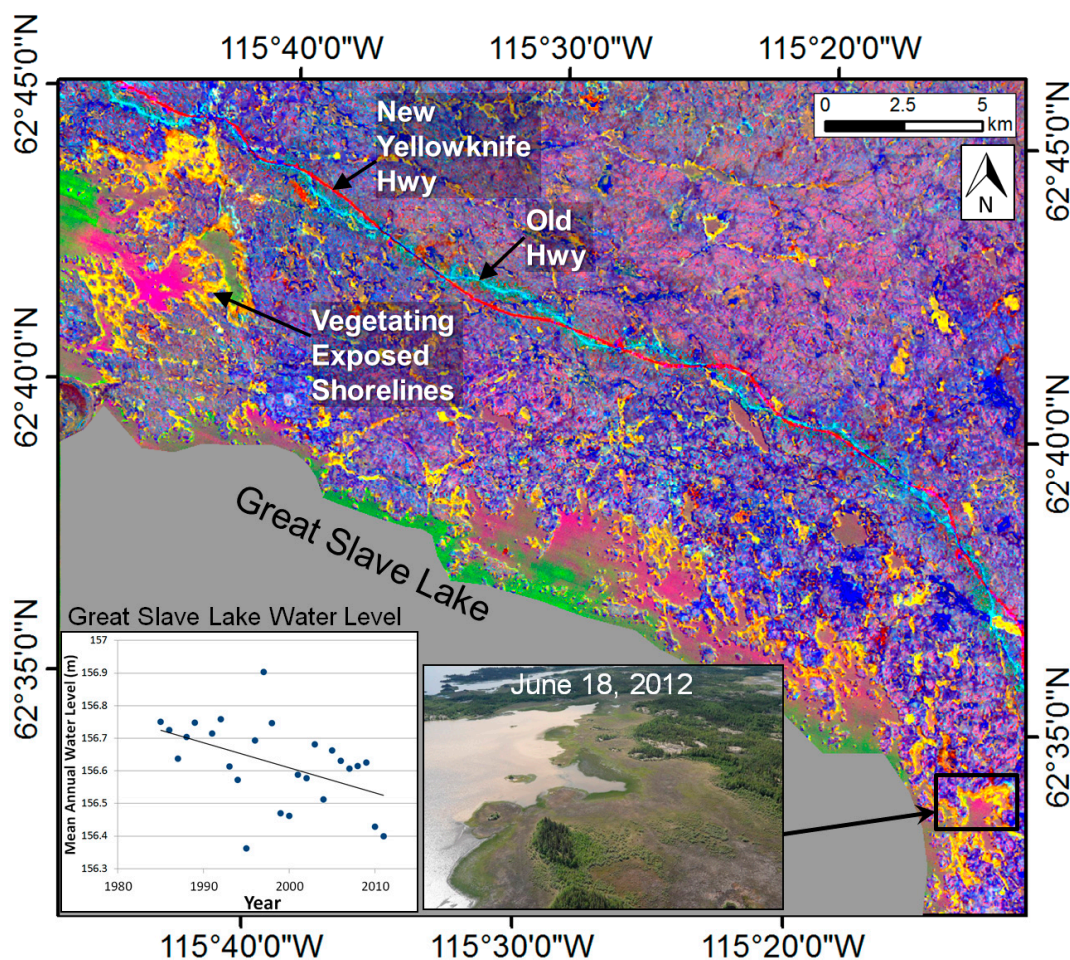


**Figure 10.** Area along the north shore of Great Slave Lake west of Yellowknife showing receding shorelines that are being colonized by vegetation in the TC trend image (yellow). The new Yellowknife Highway (red) and old highway where vegetation is regenerating (teal) are also visible. A photo captured from helicopter shows one of the bays with growth of new shoreline vegetation. Mean annual water levels from Environment Canada's Hydrometric Data are shown for Great Slave Lake at Yellowknife Bay for the 1985–2011 Landsat analysis period.

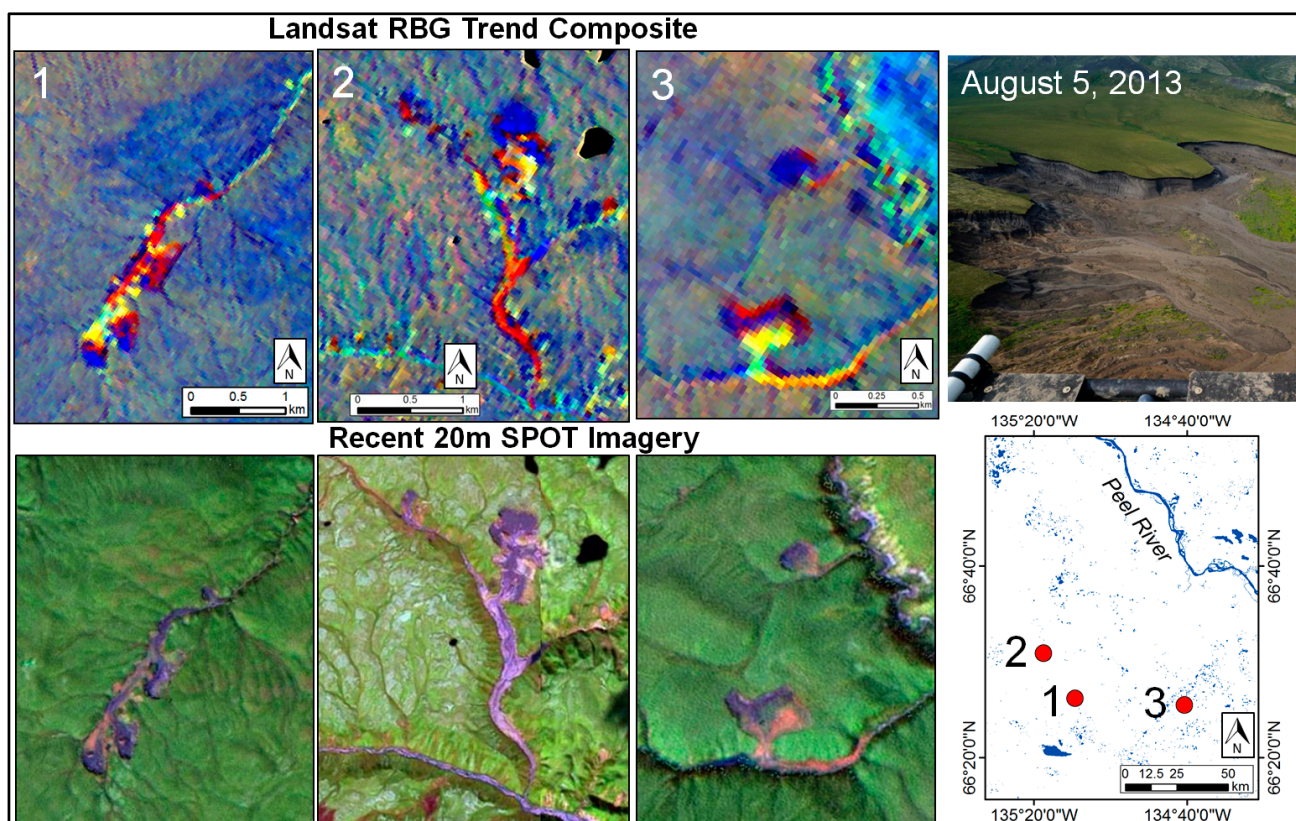


### 3.4. Retrogressive Thaw Slumps

One of the most dramatic examples of landscape change in the study regions are the retrogressive thaw slumps within the Richardson Mountains and Peel Plateau [51,52]. These thermokarst landforms occurring in ice-rich permafrost have an immense size (many >10 ha) that permits mapping them using 30 m Landsat imagery. In addition to their use in developing a regional inventory of 189 active slumps and 23 stable slumps [53], the TC trend images also provide information related to the evolution of these features (Figure 11). Active slumps comprise an ice-rich headwall, a low angle scar zone consisting of thawed sediments and debris, and in some cases, a mobile tongue of debris that develops as the saturated materials flow downslope. Growth of the slump exposes saturated sediments that contrast with adjacent tundra or forest vegetation. Once a slump stabilizes, colonizing vegetation can grow vigorously due to warm, nutrient-rich slump soils [54]. Much like regenerating wildfires, slumps follow a characteristic TC trajectory, from a wet and active portion (blue), to a dry and unvegetated surface (red), to being

stabilized and colonized by vegetation (yellow then teal) [55]. Thaw slumps occurring on lake shorelines in the Mackenzie Delta region are also observable, although with an average size of 1.3 ha [56] many approach the limit of detection using Landsat (0.4 ha) [55].

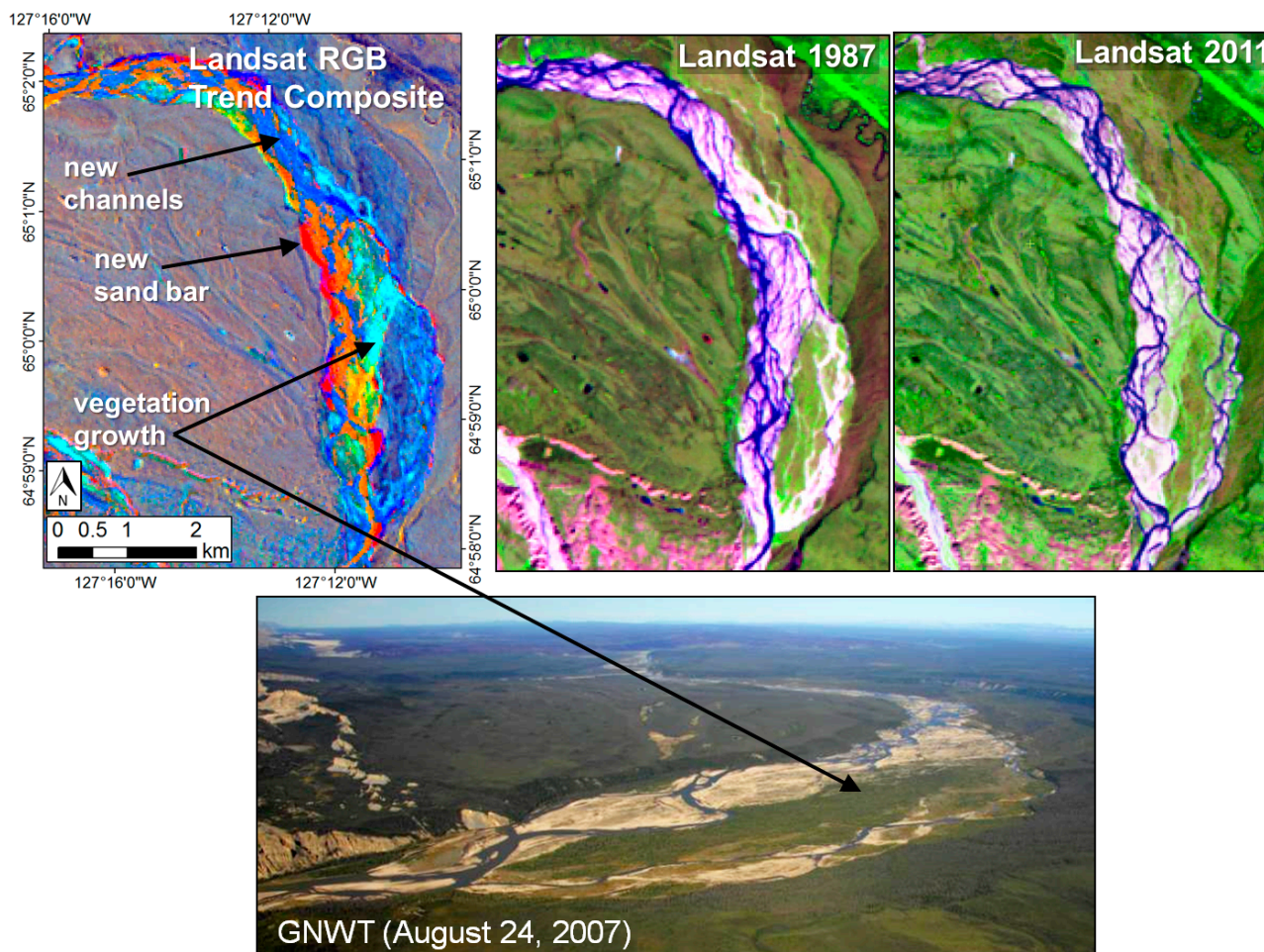
**Figure 11.** Example TC trend images for three retrogressive thaw slumps within the Peel Plateau region (**top**) with recent SPOT imagery (**bottom**) and an air photo (top right) shown for reference.



### 3.5. Fluvial Dynamics

The southern portion of study region 1 includes the foothills of the Mackenzie and Richardson Mountains and contains wide, braided river channels that provide habitat for populations of spawning char and grayling. The trend images over these areas illustrate the highly dynamic nature of shifting stream channels and the resulting changes to vegetation (Figure 12). These include transitions representing: (1) vegetation to gravel and sand bars (red) or water (dark blue); (2) water to bare gravel/sand (orange); and (3) vegetation regeneration over bare in early (light blue) or advanced (dark blue) stages.

**Figure 12.** TC trend image for a wide, braided river channel in the Mackenzie Mountain foothills west of Norman Wells (**upper left**). Comparison to single-date Landsat imagery (**upper middle, upper right**) and NWT air photos (**bottom**) show that the TC trends capture dynamic changes resulting from the shifting of stream channels and loss or gain of vegetation.

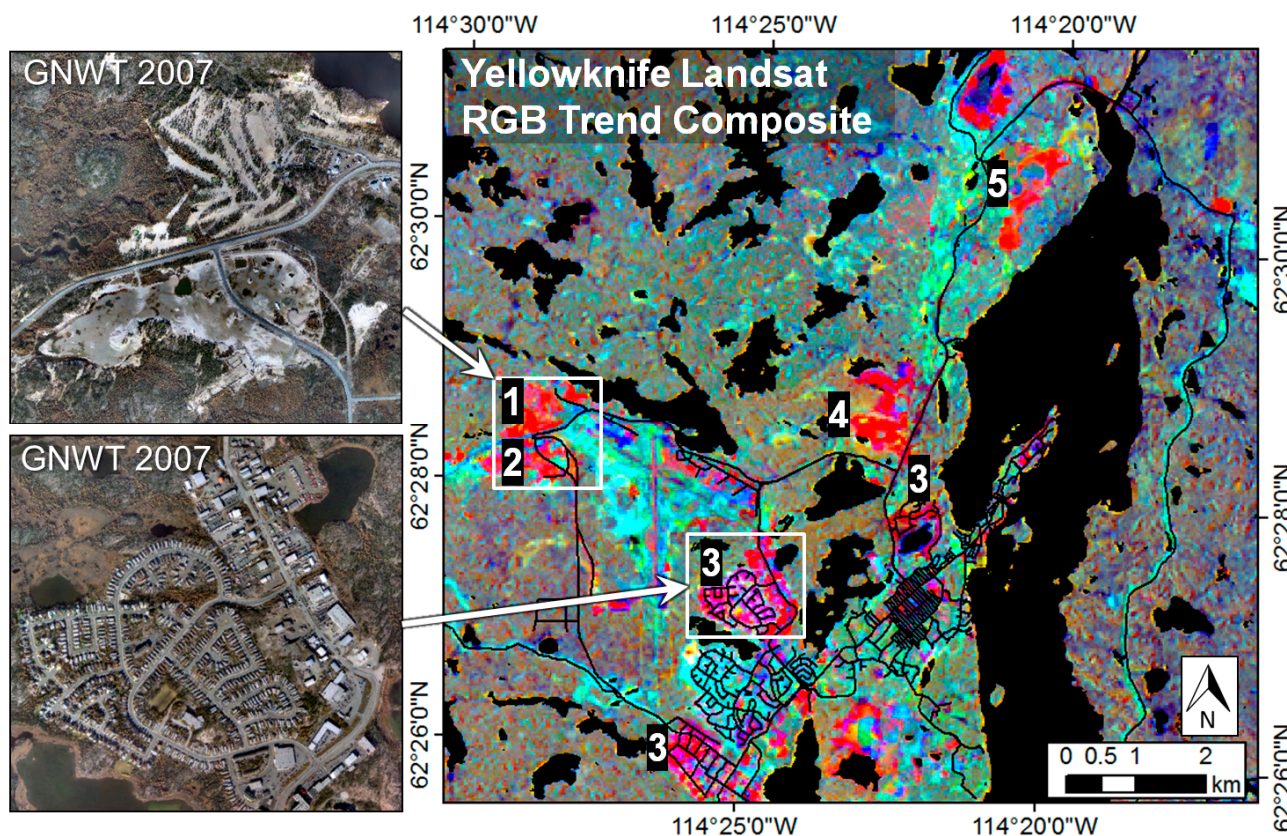


### 3.6. Mining and Anthropogenic Footprint

The NWT's economy grew rapidly during the 1985–2011 analysis period, mainly as a result of diamond mining and hydrocarbon exploration [2]. This growth has caused a wide range of land use changes that are visible in the trend composites. For example, the expanding footprints of the two largest communities in the study regions (Yellowknife and Inuvik) appear red in the trend composites. In Yellowknife (Figure 13), the conversion of vegetation to a brighter, bare surface was caused by (1) the expansion of a golf course with mostly a sand surface; (2) a gravel quarry; (3) new housing subdivisions; (4) a solid waste facility; and (5) open pits at the Giant Gold Mine.

The footprint of several mining operations in the region north of Yellowknife can also be delineated from the trend composites. Figure 14 shows two examples of non-active mines where a trend of increasing greenness and wetness (teal color) is caused by vegetation regeneration following mine abandonment. Conversely, a trend of decreasing greenness and wetness (red and purple colors) is observed where vegetation has been removed within the Ekati, Diavik, and Snap Lake diamond mine developments, which started production between 1998 and 2008.

**Figure 13.** Air photos acquired by the NWT Government in 2007 (**left**) showing land use changes visible in the TC trend image for the city of Yellowknife (**right**). These changes relate to post-1985 development (red) and regeneration of previously disturbed areas (teal) and include the construction of a golf course (1), a gravel quarry (2), new housing subdivisions (3), a solid waste facility (4), and open mining pits (5).



Linear anthropogenic disturbances can also be seen in the trend composites. Both the new Yellowknife Highway running west of Yellowknife and vegetation regeneration over the adjacent old highway are visible respectively as red and teal tones (Figure 10). Seismic line surveying leading to the removal of vegetation is the largest cumulative landscape disturbance in NWT caused by humans. Seismic lines are widely detectable in the trend imagery, despite having an average width less than 10 m, or one-third of the Landsat resolution. Strong spectral contrast produced by vigorous regeneration of broadleaf vegetation within seismic lines [57] is sufficient to make them visible throughout region 1. Figure 15 shows a highly dynamic region surrounding the town of Norman Wells, situated along the Mackenzie River. Here, a network of seismic lines is visible, along with many of the other change types discussed previously, including regenerating fires from 1955 to 2003, shifting river sand bars, draining lakes, and forest succession along the old Canol Road and pipeline built during the Second World War to transport oil to the Yukon.

**Figure 14.** Examples of TC trend imagery north of Yellowknife showing abandoned mining sites with regeneration (teal) and the footprint of recently developed diamond mines (red and dark blue).

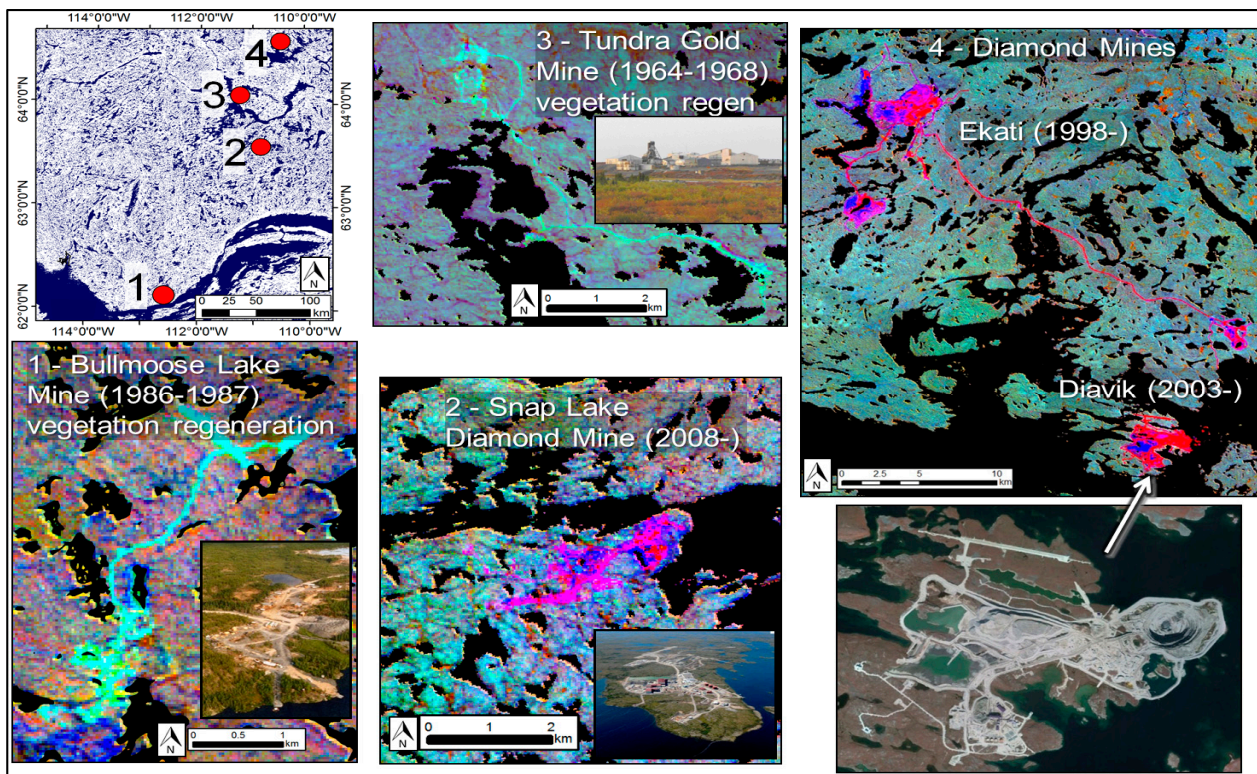
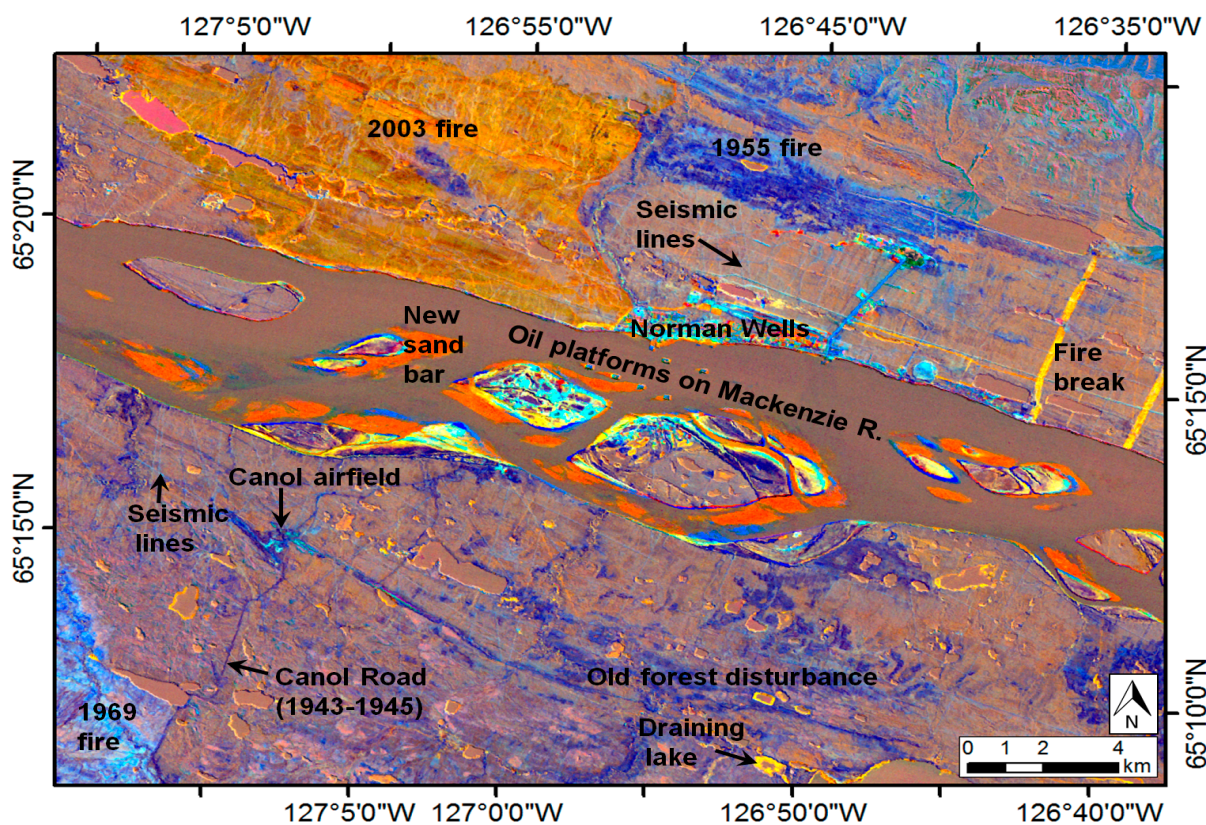


**Figure 15.** TC trend image for area surrounding Norman Wells, which has been heavily developed for oil and gas during the past 60 years.



#### 4. Discussion

The LARCH method provides a relatively simple, yet powerful means of visualizing landscape changes across large northern regions without the need to generate a categorical change classification product. We envision that environmental and land management agencies could use the trend products in a GIS environment to flag the occurrence of previously undetected landscape changes for further investigation or to quantify the nature and distribution of known disturbances. This could inform planning and decision making related to new infrastructure development (e.g., roads, quarries, buildings, and airstrips), management of ecological integrity and protected areas, and selecting sites and generating hypotheses for scientific research. The Landsat sensors appear suitable for this purpose as they provide the temporal resolution and spatial extent required to capture many of the natural and anthropogenic disturbances that are of interest to decision makers. A logical follow-on to the retrospective change analyses presented here would be to extend the image time series forward using Landsat 8 or the upcoming Sentinel-2 sensor to enable timely detection of new landscape changes.

One advantage of trend analysis approaches is that they can be used to identify subtle vegetation modifications that are not normally captured in a two-date, land cover change classification. For example, Neigh *et al.* [41] detected strong greening trends in our study area east of the Mackenzie Delta using 8 km AVHRR GIMMS imagery, but only minor Landsat-based land cover changes associated with this trend. Identification of subtle changes is made possible from a greater signal-to-noise ratio that is a result of examining multiple image dates over a long time period [11]. Examples of such changes within our study regions include the long-term succession of forest species following wildfire disturbance and tundra shrub expansion. Similarly, Landsat-based trend analysis has been found to be effective for detecting gradual and subtle changes in US forests caused by insects, drought, conifer range shifts [58], and stand-thinning [11].

Visual interpretation using the LARCH method allows the analyst to incorporate contextual information related to the change including: shape, size, texture, and geographic setting derived from overlaying ancillary GIS layers. As examples: (1) although the trends occurring within thaw slumps spectrally overlap several other types of landscape change, slumps can be readily identified based on their multiple, contiguous trends (colors) and adjacency to a stream channel (Figure 11); (2) mines are easily identified by the presence of service roads (Figure 14); (3) wildfires show a wide range of trajectories depending on their age, but are typically much larger and spatially homogeneous than other landscape changes (Figure 4); and (4) changes in lake area can be tracked with reference to a database of historical lake extents (Figure 9). The interpretation of changes is also aided by the physical nature of the Tasseled Cap BGW transformations, which allows colors or queried slope values in the composite image to be related to physical characteristics of the changes. For example, a red color generated by increasing TC brightness, and decreasing TC greenness and wetness is normally associated with the conversion of mature forest stands to a bare surface [59].

The major limitation of characterizing changes using linear trends is that many change processes, such as fires and slumps, have distinctly non-linear spectral-temporal trajectories [35]. Despite this simplification, linear regression analysis does generate characteristic trends related to disturbance age and evolution. The addition of higher-order functions could be used to better represent non-linear change processes, but this would require more complex means of visualization [12]. Another limitation of the

LARCH visualization approach is that it does not generate a digital map product that delineates and classifies change objects for follow-on statistical or other quantitative analyses. Change patches can be manually digitized on-screen or thresholded in TC trend space, but this would not be practical for large areas. Both of these limitations are addressed in a companion paper in this issue [36] that investigates the use of curve profile matching and non-linear functions in decision tree classifiers to produce change classification maps that complement the visual trend products.

## 5. Conclusions

Linear trend analysis of the Tasseled Cap brightness, greenness, and wetness indices from a long-term (1985–2011) record of near-annual, growing-season Landsat images provides a simple, yet powerful means of visualizing landscape disturbances in northern environments. When regression slope coefficients from the three indices are composited into an RGB image, this generates a unique color representing the three dimensional Tasseled Cap trajectory. A wide range of landscape-scale changes can thus be distinguished, including wildfire regeneration, tundra greening, thermokarst processes, and disturbance resulting from resource development operations.

The LARCH method is limited by the fact that many types of disturbances (e.g., wildfire) follow a non-linear reflectance trajectory, which can make linear slope coefficients difficult to interpret. Slopes computed from a long-term time series are also insensitive to changes occurring at later dates where only a limited number of observations will reflect the changed state. Despite these simplifications, RGB color composites produced using this method provide an effective means of documenting the occurrence and likely cause of landscape changes without the benefit of ground-based information. The approach can therefore complement more quantitative change classification methods and is well-suited for remote northern regions when ground-based monitoring is not practical.

## Acknowledgements

We thank Marilee Pregitzer and Alice Deschamps for assistance with satellite image and GIS processing. Vern Singhroy and Christian Prevost from CCMEQ and our anonymous reviewers offered helpful comments to improve the paper. The Polar Continental Shelf Program of Natural Resources Canada provided helicopter time from Great Slave Helicopters to acquire air photos. Funding for this work was provided by Natural Resources Canada's TRACS project led by Stephen Wolfe and by the NWT Cumulative Impacts Monitoring Program under the projects "A Multi-scale Assessment of Cumulative Impacts in the Northern Mackenzie Basin" led by Claire Marchildon and "A watershed approach to monitoring cumulative impacts of landscape change" led by Krista Chin.

## Author Contributions

Robert Fraser wrote the first draft of the manuscript and was responsible for the research design and leading the data analysis. All authors supported the interpretation of the results and contributed to writing and editing the manuscript. Alexander Brooker prepared the Landsat data for analysis. Trevor Lantz, Denis Lacelle, Steven Kokelj, Ian Olthof, and Stephen Wolfe contributed to field and helicopter surveys.

## Conflicts of Interest

The authors declare no conflict of interest.

## References

1. Arctic Climate Impact Assessment (ACIA). *Arctic Climate Impact Assessment*; Cambridge University Press: Cambridge, UK, 2005.
2. SENES Consultants Limited (SENES). Northwest Territories Environmental Audit 2005. Available online: <https://www.aadnc-aandc.gc.ca/eng/1100100027504/1100100027505> (accessed on 7 November 2014).
3. Plug, L.J.; Walls, C.; Scott, B.M. Tundra lake changes from 1978 to 2001 on the Tuktoyaktuk Peninsula, western Canadian Arctic. *Geophys. Res. Lett.* **2008**, *35*, L03502.
4. Labrecque, S.; Lacelle, D.; Duguay, C.R.; Lauriol, B.; Hawkings, J. Contemporary (1951–2001) evolution of lakes in the Old Crow Basin, Northern Yukon, Canada: Remote sensing, numerical modeling, and stable isotope analysis. *Arctic* **2009**, *62*, 225–238.
5. Lantz, T.C.; Kokelj, S.V.; Fraser, R.H. Ecological recovery in an arctic delta following widespread saline incursion. *Ecol. Appl.* **2014**, in press.
6. Dowdeswell, E.K.; Dowdeswell, J.A.; Cawkwell, F. On the glaciers of Bylot Island, Nunavut, Arctic Canada. *Arct. Antarct. Alp. Res.* **2007**, *39*, 402–411.
7. Pouliot, D.; Latifovic, R.; Olthof, I. Trends in vegetation NDVI from 1 km AVHRR data over Canada for the period 1985–2006. *Int. J. Remote Sens.* **2009**, *30*, 149–168.
8. Epp, H.; Lanoville, R. Satellite data and geographic information systems for fire and resource management in the Canadian arctic. *Geocarto Int.* **1996**, *11*, 97–103.
9. Fraser, R.H.; Li, Z.; Cihlar, J. Hotspot and NDVI Differencing Synergy (HANDS): A new technique for burned area mapping over Boreal forest. *Remote Sens. Environ.* **2000**, *74*, 362–376.
10. Ichoku, C.; Kaufman, Y.J.; Giglio, L.; Li, Z.; Fraser, R.H.; Jin, J.-Z.; Park, W.M. Comparative analysis of daytime fire detection algorithms using AVHRR data for the 1995 fire season in Canada: Perspective for MODIS. *Int. J. Remote Sens.* **2003**, *24*, 1669–1690.
11. Kennedy, R.E.; Cohen, W.B.; Schroeder, T.A. Trajectory-based change detection for automated characterization of forest disturbance dynamics. *Remote Sens. Environ.* **2007**, *110*, 370–386.
12. Lehmann, E.A.; Wallace, J.F.; Caccetta, P.A.; Furby, S.L.; Zdunic, K. Forest cover trends from time series Landsat data for the Australian continent. *Int. J. Appl. Earth Obs. Geoinf.* **2013**, *21*, 453–462.
13. Kennedy, R.E.; Yang, Z.; Cohen, W.B.; Pfaff, E.; Braaten, J.; Nelson, P. Spatial and temporal patterns of forest disturbance and regrowth within the area of the Northwest Forest Plan. *Remote Sens. Environ.* **2012**, *122*, 117–133.
14. Huang, C.; Goward, S.N.; Masek, J.G.; Thomas, N.; Zhu, Z.; Vogelmann, J.E. An automated approach for reconstructing recent forest disturbance history using dense Landsat time series stacks. *Remote Sens. Environ.* **2010**, *114*, 183–198.
15. Zhu, Z.; Woodcock, C.E. Continuous change detection and classification of land cover using all available Landsat data. *Remote Sens. Environ.* **2014**, *144*, 152–171.

16. Olthof, I.; Pouliot, D. Recent (1986–2006) vegetation-specific NDVI trends in northern Canada from satellite data. *Arctic* **2008**, *61*, 381–394.
17. Fraser, R.H.; Olthof, I.; Carrière, M.; Deschamps, A.; Pouliot, D. Detecting long-term changes to vegetation in northern Canada using the Landsat satellite image archive. *Environ. Res. Lett.* **2011**, *6*, 045502.
18. McManus, K.M.; Morton, D.C.; Masek, J.G.; Wang, D.; Sexton, J.O.; Nagol, J.R.; Ropars, P.; Boudreau, S. Satellite-based evidence for shrub and graminoid tundra expansion in northern Quebec from 1986 to 2010. *Glob. Chang. Biol.* **2012**, *18*, 2313–2323.
19. Reynolds, M.K.; Walker, D.A.; Verbyla, D.; Munger, C.A. Patterns of change within a tundra landscape: 22-year Landsat NDVI trends in an area of the northern foothills of the Brooks Range, Alaska. *Arct. Antarct. Alp. Res.* **2013**, *45*, 249–260.
20. Rover, J.; Ji, L.; Wylie, B.K.; Tieszen, L.L. Establishing water body areal extent trends in interior Alaska from multi-temporal Landsat data. *Remote Sens. Lett.* **2012**, *3*, 595–604.
21. Fraser, R.H.; Lantz, T.C.; Olthof, I.; Kokelj, S.V.; Sims, R.A. Warming-induced shrub expansion and lichen decline in the Western Canadian Arctic. *Ecosystems* **2014**, *17*, 1151–1168.
22. Timoney, K.P.; la Roi, G.H.; Zoltai, S.C.; Robinson, A.L. The high subarctic forest-tundra of northwestern Canada: Position, width, and vegetation gradients in relation to climate. *Arctic* **1992**, *45*, 1–9.
23. Ecosystem Classification Group. *Ecological Regions of the Northwest Territories—Southern Arctic*; Department of Environment and Natural Resources, Government of the Northwest Territories: Yellowknife, NT, Canada, 2012.
24. Burn, C.R.; Kokelj, S.V. The environment and permafrost of the Mackenzie Delta area. *Permafr. Periglac. Process.* **2009**, *20*, 83–105.
25. Smith, S.L.; Romanovsky, V.E.; Lewkowicz, A.G.; Burn, C.R.; Allard, M.; Clow, G.D.; Yoshikawa, K.; Throop, J. Thermal state of permafrost in north America: A contribution to the international polar year. *Permafr. Periglac. Process.* **2010**, *21*, 117–135.
26. Kokelj, S.V.; Jorgenson, M.T. Advances in thermokarst research. *Permafr. Periglac. Process.* **2013**, *24*, 108–119.
27. Lantz, T.C.; Marsh, P.; Kokelj, S.V. Recent shrub proliferation in the Mackenzie Delta Uplands and microclimatic implications. *Ecosystems* **2012**, *16*, 47–59.
28. Rosenberg International Forum on Water Policy. Rosenberg International Forum: The Mackenzie Basin. 2013. Available online: <http://ciwr.ucanr.edu/files/168679.pdf> (accessed on 7 November 2014).
29. Chander, G.; Markham, B.L.; Helder, D.L. Summary of current radiometric calibration coefficients for Landsat MSS, TM, ETM+, and EO-1 ALI sensors. *Remote Sens. Environ.* **2009**, *113*, 893–903.
30. Crist, E.P.; Cicone, R.C. A physically-based transformation of thematic mapper data—The TM tasseled cap. *IEEE Trans. Geosci. Remote Sens.* **1984**, *GE-22*, 256–263.
31. Kendall, M.G.; Stuart, A.S. *Advanced Theory of Statistics*; Charles Griffin and Company: London, UK, 1967; Volume 2.
32. Coppin, P.; Jonckheere, I.; Nackaerts, K.; Muys, B.; Lambin, E. Digital change detection methods in ecosystem monitoring: A review. *Int. J. Remote Sens.* **2004**, *25*, 1565–1596.

33. Kasischke, E.S.; French, N.H.F.; Bourgeau-Chavez, L.L.; Michalek, J.L. Using satellite data to monitor fire-related processes in boreal forests. In *Fire, Climate Change, and Carbon Cycling in the Boreal Forest*; Kasischke, E.S., Stocks, B.J., Eds.; Ecological Studies; Springer: New York, NY, USA, 2000; pp. 406–422.
34. Hollingsworth, T.N.; Johnstone, J.F.; Bernhardt, E.L.; Chapin, F.S., III. Fire severity filters regeneration traits to shape community assembly in Alaska's boreal forest. *PLoS One* **2013**, *8*, e56033.
35. Song, C.; Woodcock, C.E.; Li, X. The spectral/temporal manifestation of forest succession in optical imagery—The potential of multitemporal imagery. *Remote Sens. Environ.* **2002**, *82*, 285–302.
36. Olthof, I.; Fraser, R.H. Detecting landscape change in high latitude environments using Landsat trend analysis: 2. Classification. *Remote Sens.* **2014**, doi:10.3390/rs61111558.
37. Cody, W.J. *Reindeer Range Survey 1957 and 1963*; Plant Research Institute, Canada, Department of Agriculture, Central Experimental Farm: Ottawa, ON, Canada, 1964.
38. Mack, M.C.; Bret-Harte, M.S.; Hollingsworth, T.N.; Jandt, R.R.; Schuur, E.A.G.; Shaver, G.R.; Verbyla, D.L. Carbon loss from an unprecedented Arctic tundra wildfire. *Nature* **2011**, *475*, 489–492.
39. Myers-Smith, I.H.; Forbes, B.C.; Wilmking, M.; Hallinger, M.; Lantz, T.; Blok, D.; Tape, K.D.; Macias-Fauria, M.; Sass-Klaassen, U.; Lévesque, E.; *et al.* Shrub expansion in tundra ecosystems: Dynamics, impacts and research priorities. *Environ. Res. Lett.* **2011**, *6*, 045509.
40. Goetz, S.J.; Bunn, A.G.; Fiske, G.J.; Houghton, R.A. Satellite-observed photosynthetic trends across boreal North America associated with climate and fire disturbance. *Proc. Natl. Acad. Sci. USA* **2005**, *102*, 13521–13525.
41. Neigh, C.S.R.; Tucker, C.J.; Townshend, J.R.G. North American vegetation dynamics observed with multi-resolution satellite data. *Remote Sens. Environ.* **2008**, *112*, 1749–1772.
42. Chapin, F.S.; Sturm, M.; Serreze, M.C.; McFadden, J.P.; Key, J.R.; Lloyd, A.H.; McGuire, A.D.; Rupp, T.S.; Lynch, A.H.; Schimel, J.P.; *et al.* Role of land-surface changes in Arctic summer warming. *Science* **2005**, *310*, 657–660.
43. Riordan, B.; Verbyla, D.; McGuire, A.D. Shrinking ponds in subarctic Alaska based on 1950–2002 remotely sensed images. *J. Geophys. Res.* **2006**, *111*, G04002.
44. Roach, J.K.; Griffith, B.; Verbyla, D. Landscape influences on climate-related lake shrinkage at high latitudes. *Glob. Chang. Biol.* **2013**, *19*, 2276–2284.
45. Jones, B.M.; Grosse, G.; Arp, C.D.; Jones, M.C.; Walter Anthony, K.M.; Romanovsky, V.E. Modern thermokarst lake dynamics in the continuous permafrost zone, northern Seward Peninsula, Alaska. *J. Geophys. Res.* **2011**, *116*, G00M03.
46. Yoshikawa, K.; Hinzman, L.D. Shrinking thermokarst ponds and groundwater dynamics in discontinuous permafrost near council, Alaska. *Permafr. Periglac. Process.* **2003**, *14*, 151–160.
47. Mackay, J.R. Pingo growth and collapse, Tuktoyaktuk Peninsula area, western Arctic coast, Canada: A long-term field study. *Géogr. Phys. Quat.* **1998**, *52*, 271–323.
48. Mackay, J.R. Periglacial features developed on the exposed lake bottoms of seven lakes that drained rapidly after 1950, Tuktoyaktuk Peninsula area, western arctic coast, Canada. *Permafr. Periglac. Process.* **1999**, *10*, 39–63.

49. Jorgenson, M.T.; Shur, Y.L.; Pullman, E.R. Abrupt increase in permafrost degradation in arctic Alaska. *Geophys. Res. Lett.* **2006**, *33*, L02503.
50. Solomon, S.M. Spatial and temporal variability of shoreline change in the Beaufort-Mackenzie region, northwest Territories, Canada. *Geo-Mar Lett.* **2005**, *25*, 127–137.
51. Lacelle, D.; Bjornson, J.; Lauriol, B. Climatic and geomorphic factors affecting contemporary (1950–2004) activity of retrogressive thaw slumps on the Aklavik Plateau, Richardson Mountains, NWT, Canada. *Permafr. Periglac. Process.* **2010**, *21*, 1–15.
52. Kokelj, S.V.; Lacelle, D.; Lantz, T.C.; Tunnicliffe, J.; Malone, L.; Clark, I.D.; Chin, K.S. Thawing of massive ground ice in mega slumps drives increases in stream sediment and solute flux across a range of watershed scales. *J. Geophys. Res. Earth Surf.* **2013**, *118*, 681–692.
53. Lacelle, D.; Brooker, A.; Fraser, R.H.; Kokelj, S.V. Effect of terrain factors and solar radiation on the distribution and growth of thaw slumps (1985–2011) in the Richardson Mountains—Peel Plateau region, northwestern Canada. *Geomorphology* **2014**, submitted.
54. Lantz, T.C.; Kokelj, S.V.; Gergel, S.E.; Henry, G.H.R. Relative impacts of disturbance and temperature: Persistent changes in microenvironment and vegetation in retrogressive thaw slumps. *Glob. Chang. Biol.* **2009**, *15*, 1664–1675.
55. Brooker, A.; Fraser, R.H.; Olthof, I.; Kokelj, S.V.; Lacelle, D. Tasseled Cap trend analysis of a Landsat satellite image stack (1985–2011): A method to track the life cycle of retrogressive thaw slumps at high temporal resolution. *Permafr. Periglac. Process.* **2014**, in press.
56. Lantz, T.C.; Kokelj, S.V. Increasing rates of retrogressive thaw slump activity in the Mackenzie Delta region, N.W.T., Canada. *Geophys. Res. Lett.* **2008**, *35*, L06502.
57. Kemper, J.T.; Macdonald, S.E. Directional change in upland tundra plant communities 20–30 years after seismic exploration in the Canadian low-arctic. *J. Veg. Sci.* **2009**, *20*, 557–567.
58. Vogelmann, J.E.; Xian, G.; Homer, C.; Tolk, B. Monitoring gradual ecosystem change using Landsat time series analyses: Case studies in selected forest and rangeland ecosystems. *Remote Sens. Environ.* **2012**, *122*, 92–105.
59. Healey, S.P.; Cohen, W.B.; Yang, Z.; Krankina, O.N. Comparison of Tasseled Cap-based Landsat data structures for use in forest disturbance detection. *Remote Sens. Environ.* **2005**, *97*, 301–310.